https://doi.org/10.5194/egusphere-2026-5070
Preprint. Discussion started: 31 August 2026

Sea-ice thickness initialization improves summertime sea ice prediction in the Barents-Kara Sea

Yushi Morioka[1], Doroteaciro Iovino[2], Andrea Cipollone[2], Andrea Storto[3], Takeshi Doi[1], Masami Nonaka[1], Swadhin K. Behera[1]

1: Japan Agency for Marine-Earth Science and Technology
2: Institute for Earth System Predictions, CMCC
3: Institute of Marine Sciences, CNR

Corresponding Author: Yushi Morioka
Showamachi 3173-25, Kanazawa-ku, Yokohama, JAPAN
morioka@jamstec.go.jp, +81-45-778-5509

https://doi.org/10.5194/egusphere-2026-5070
Preprint. Discussion started: 31 August 2026

Abstract

Arctic sea ice has substantially declined over the past four decades. Given the projected decrease under global warming, reliable prediction of summer sea ice is becoming increasingly important. Yet most climate models still show limited low skill in predicting summer sea ice from spring, a limitation commonly referred to as the spring predictability barrier. Here we develop a seasonal forecast system based on an eddy-permitting coupled model and assess how different ocean and sea ice initialization strategies affect prediction skill. Results show that the summer sea ice in the Barents-Kara Sea is predicted most skillfully when sea ice and snow conditions in the model are initialized. Sea ice initialization improves the representation of the initial sea ice thickness, the subsequent ice-albedo feedback, and the meridional sea ice advection from the higher latitudes. These findings suggest significance of sea ice thickness initialization for skillful summer prediction despite the spring predictability barrier.

https://doi.org/10.5194/egusphere-2026-5070
Preprint. Discussion started: 31 August 2026

1. Introduction

Arctic sea ice extent (SIE; see Methods) has substantially declined over the past few decades (Cavalieri and Parkinson, 2012), although the rate of SIE decline has slowed down in the last decade (Zhang, 2015; Zhang, 2021; Wang et al., 2025). Amid global warming, Arctic SIE is expected to continue decreasing (Boé et al., 2009; Wang and Overland, 2009, 2012; Notz and Community, 2020; Jahn et al., 2024) with significant consequences on regional weather and climate (Vihma, 2014), and marine biogeochemistry and ecosystems (Lannuzel et al., 2020). Reduced sea ice cover facilitates human access to Arctic marginal seas, creating new opportunities for socioeconomic activities such as fishery (Christiansen et al., 2014), shipping (Melia et al., 2016), natural resource exploitation (Meier et al., 2014), and ecotourism (Palma et al., 2019). For commercial use, seasonal prediction of Arctic SIE during boreal summer (July-September) when the SIE reaches its annual minimum (Fig. 1a) is highly needed (Guemas et al., 2016; Holland and Hunke, 2022).

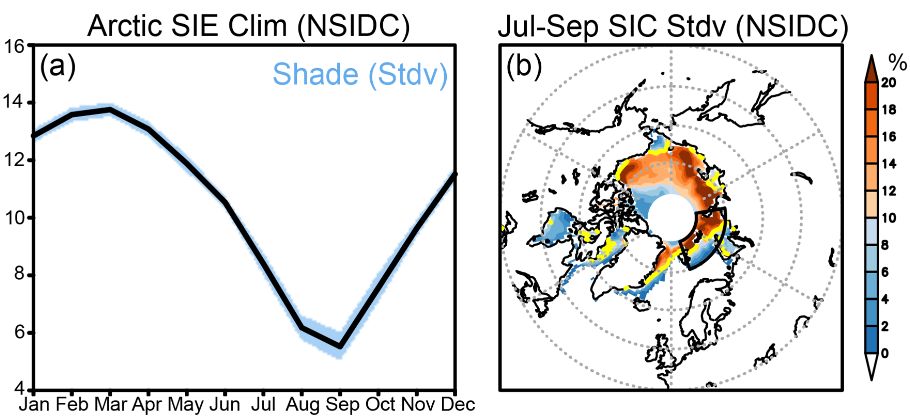

Figure 1: (a) Monthly climatology of Arctic SIE (black solid line; in 10^6 km^2) during 1982-2022 from NSIDC. Shade indicates one and minus one standard deviation of Arctic SIE. (b) July-September SIC standard deviation (Stdv; color in %) in the Arctic Ocean. Yellow line corresponds to the sea ice edge with July-September SIC climatology of 15 %. Black curved box indicates the Barents-Kara Sea of interest.

Arctic sea ice concentration (SIC) undergoes a large interannual variability near the sea ice edge (Fig. 1b). Atmosphere-ocean coupled model simulations demonstrate that spring ice-albedo feedback plays a key role in shaping summer sea ice variability through changes in the sea ice albedo and absorption/reflection of incoming solar radiation, alongside contributions

https://doi.org/10.5194/egusphere-2026-5070
Preprint. Discussion started: 31 August 2026

from horizontal sea ice transport inherited from winter conditions (Bushuk et al., 2020). However, most coupled models (Bushuk et al., 2017, 2019; Bonan et al., 2019) show limited skill in predicting summer sea ice from May or June, a limitation referred to as "spring predictability barrier (Day et al., 2014a)". This barrier is likely due to misrepresentation of the initial states, especially initial sea ice thickness (SIT; Day et al., 2014b; Guemas et al., 2016; Dirkson et al., 2017; Ono et al., 2020; Zhang et al., 2023; Song et al., 2024; Liu et al., 2025), which provides seasonal memory for SIC anomalies. Additional contributions may come from sea ice model physics (Massonnet et al., 2011) and insufficient model resolutions (Selivanova et al., 2024). None of the coupled models have adopted SIT initialization in the operational seasonal prediction (Blockley and Peterson, 2018; Batté et al., 2020; Balan-Sarojini et al., 2021), due to a short SIT observation record from 2010.

To overcome the spring predictability barrier, we explore the impacts of ocean and sea ice initializations on prediction skill of Arctic sea ice, using a seasonal prediction system based on the eddy-permitting coupled model SINTEX-F3 (see Methods), which has a nominal horizontal resolution of 25 km in the ocean and sea ice components. By comparing with other eddy-permitting coupled models from C3S (see Methods), we demonstrate that initializing sea ice, particularly SIT, is essential for overcoming the spring predictability barrier in the Barents-Kara Sea. The prediction skills with sea ice (SIC, SIT, and snow depth) initialization are higher than those with ocean (sea surface temperature, and subsurface ocean temperature and salinity) initializations. These results underscore the significance of sea ice initialization for seasonal prediction of summer sea ice in the Barents-Kara Sea and highlight the need of long-term SIT observation in the region.

2. Methods

2.1. Observation data and reanalysis products

We used daily sea ice concentration (SIC) data at 25 km horizontal resolution during 1982-2022 from National Snow and Ice Data Center (NSIDC), based on Nimbus-7 SMMR and DMSP SSM/I-SSMIS Passive Microwave Data Version 2 (DiGirolamo et al., 2022). We also employed monthly sea ice thickness reanalysis at 0.25° horizontal resolution from Euro-Mediterranean Center on Climate Change (CMCC) Global Ocean Reanalysis Systems (C-GLORS; Storto and Masina, 2016; Cipollone et al., 2023). Sea ice extent (SIE) was defined as the total surface area with the SIC greater than 15%, and sea ice area (SIA) as the sum of grid-cell area multiplied by the SIC. For the ocean, we used monthly sea surface temperature (SST)

https://doi.org/10.5194/egusphere-2026-5070
Preprint. Discussion started: 31 August 2026

data at 0.25º horizontal resolution from National Oceanic and Atmospheric Administration (NOAA) and based on the optimal interpolation SST analysis version 2 (OISSTv2) high-resolution dataset (Reynolds et al., 2007). We also utilized monthly subsurface ocean temperature and salinity objective analysis data at 1º horizontal resolution from UK's Met Office and based on EN4 (Good et al., 2013). For the atmosphere, we analyzed monthly surface winds at 10 m, and surface heat flux at 0.25º horizontal resolution from European Center for Medium-Range Weather Forecasts (ECMWF) and based on the fifth generation ECMWF reanalysis (ERA5; Hersbach et al., 2020). All observational and reanalysis products were interpolated to a common 1ºx1º grid for comparison with the model simulations.

2.2. Seasonal reforecasts based on SINTEX-F models

We adopted two atmosphere-ocean coupled models developed at Japan Agency for Marine-Earth Science and Technology (JAMSTEC) under EU-Japan collaboration. We employ the second generation of Scale Interaction Tropical Experiment-Frontier (SINTEX-F2; Masson et al., 2012; Sasaki et al., 2013) model for the eddy-parameterized coupled model. The oceanic component of SINTEX-F2 is based on the Nucleus for European Modeling of the Ocean (NEMO3.4; Madec et al., 2008) system, which comprises the Ocean Parallelise (OPA9) ocean model and the Louvain-la-Neuve sea ice model (LIM2; Fichefet and Maqueda, 1997) at a nominal horizontal resolution of 0.5º, with 31 vertical levels in the rescaled z* height coordinate. Its atmospheric component is based on the 5th version of the ECMWF and Max Planck Institute for Meteorology (MPI-M) in the Hamburg atmospheric model (ECHAM5.4; Roeckner et al., 2003). ECHAM5.4 has a horizontal resolution of T106 (approximately 125 km at the equator) with 31 vertical levels of up to 1 hPa and adopts a sophisticated parameterization for cumulous convection (Nordeng et al., 1994). Surface heat flux, momentum, and freshwater for the atmosphere and ocean were exchanged every two hours with no flux correction, using the third version of the Ocean Atmosphere Sea Ice Soil coupler (OASIS3; Valcke et al., 2004).

For comparison, we used the third version of the eddy-permitting SINTEX-F (SINTEX-F3) model. Its oceanic component is based on the NEMO4.0 system (Madec et al., 2019), coupled to the SI^3 sea ice model (Vancoppenolle et al., 2023) at a nominal horizontal resolution of 0.25º with 75 vertical levels in the rescaled z* height coordinate. Its atmospheric component is based on the 6th version of the ECMWF and MPI-M in the Hamburg atmospheric model (ECHAM6; Giorgetta et al., 2013), which has a horizontal resolution of T255 (approximately 60 km at the equator) with 95 vertical levels up to 0.01 hPa and adopts the same

https://doi.org/10.5194/egusphere-2026-5070
Preprint. Discussion started: 31 August 2026

parameterization for cumulous convection (Nordeng et al., 1994). The major differences between ECHAM5 and ECHAM6 involve land processes that are based on the land vegetation Jena Scheme for Biosphere Atmosphere Coupling (JSBACH; Raddatz et al., 2007), modified radiation schemes, computation of the surface albedo, and the triggering conditions required for convection. The surface heat flux, momentum, and freshwater between the atmosphere and ocean were exchanged every one hour with no flux correction using the OASIS coupler interfaced with the Model Coupling Toolkit (OASIS-MCT) coupler (Valcke et al., 2013).

We spun up both SINTEX-F2 and SINTEX-F3 for 31 years from the initial conditions under the pre-industrial radiative forcings. In SINTEX-F2, the ocean model was initialized using monthly ocean temperature and salinity climatologies in January from the Levitus dataset (Levitus, 1982) with no motion, whereas in SINTEX-F3, the ocean model was initialized using the monthly ocean temperature and salinity climatologies in January from the World Ocean Atlas 2013 dataset (WOA13; Locarnini et al., 2013; Zweng et al., 2013) with no motion. Then, we initialized the model SST using the two observed SST datasets from OISSTv2 low-resolution (1^{o}; Reynolds et al., 2002) and high-resolution (0.25^{o}; Reynolds et al., 2007) datasets. We restored the model SST every timestep during 1982-2022 by adding the surface heat flux for the difference with the observed SST using three different nudging strengths (800, 1200, and 2400 W m^{-2}/K). This generates six ensemble members (i.e., two SST datasets times three nudging strengths) for the SST initialization. For the SINTEX-F3, we added sea ice initialization in which the model SIC, SIT, and snow depth are restored to the sea ice reanalysis from C-GLORS on the first day of every month. This leads to six additional ensemble members for the SST and sea ice initializations. Furthermore, we added subsurface ocean temperature and salinity initialization via a three-dimensional variational data assimilation (3DVAR; Storto et al., 2018) approach in which the model temperature and salinity are assimilated to the profile data from EN4 using the incremental analysis update (IAU; Bloom et al., 1996) over the time window of the first 10 days of every month. This also produces six ensemble members for the SST, sea ice, and subsurface ocean initializations. We conducted seasonal reforecasts from May 1st of every year during the period of 1982-2022 with a lead time of one year in which the models are freely integrated. This results in six ensemble members for each of the SINTEX-F2 seasonal forecasts with the SST initialization (F2-SST), the SINTEX-F3 seasonal forecasts with the SST initialization (F3-SST), the SST and sea ice initialization (F3-SI), and the SST, sea ice, and subsurface ocean initializations (F3-3DVAR). We removed model drift by calculating the differences between the observed and model climatologies and subtracted monthly climatology and linear trend using a least squares method to derive monthly anomalies.

https://doi.org/10.5194/egusphere-2026-5070
Preprint. Discussion started: 31 August 2026

2.3. Seasonal reforecasts based on C3S models

We adopted seasonal reforecasts based on other coupled models, which are provided through the Copernicus Climate Change Service (C3S). Due to the data availability, we analyzed the seasonal reforecasts from May 1st, which are based on ACCESS-S2 (Wedd et al., 2022) from the Australian Bureau of Meteorology (BOM), CMCC-SPS4 (Sanna et al., 2025) from the Euro-Mediterranean Center on Climate Change (CMCC), GCFS2.2 (Fröhlich et al., 2020) from the German Weather Service (DWD), GEM5.2-NEMO (Diro et al., 2024) from Environment and Climate Change Canada (ECCC), SEAS5 (Stockdale, 2021) from European Center for Medium-Range Weather Forecasts (ECMWF), Météo-France System 9 (Specq et al., 2025) from Météo-France (METEOFR), GloSea6-GC3.2 (Williams et al., 2017) from UK's Met Office (UKMO). A summary of seasonal reforecast systems is provided in Table 1. To make fair comparison with SINTEX-F models, we analyzed seasonal reforecasts based on C3S models during 1993-2016. We also removed model drift and linear trend to calculate monthly anomalies in a similar manner to SINTEX-F models.

Table 1: Description of seasonal reforecast systems

Name	**Atm-Lnd**	**Ocn-Ice**	**Init**	**Period**	**Ens**	**Lead**
BOM	60 km, L85	25 km, L75	Atm, Lnd, Ocn	1983-2018	27	6
CMCC	50 km, L83	25 km, L75	Atm, Lnd, Ocn	1993-2022	30	6
DWD	100 km, L95	40 km, L40	Atm, Ocn, Ice (SIC)	1993-2023	30	6
ECCC	50 km, L85	100 km, L50	Atm, Lnd, Ocn	1993-2025	20	6
ECMWF	40 km, L91	25 km, L75	Atm, Lnd, Ocn	1981-2025	25	6
METEOFR	50 km, L137	25 km, L75	Atm, Lnd, Ocn	1993-2025	31	6
UKMO	60 km, L85	25 km, L75	Atm, Lnd, Ocn	1993-2016	28	6
SINTEX-F2	100 km, L31	100 km, L31	Ocn	1982-2023	6	12
SINTEX-F3	60 km, L95	25 km, L75	Ocn, Ice (SIC, SIT, Snow)	1982-2023	18	12

Note: From left to right, agency/model name, horizontal and vertical resolutions for atmosphere and land surface models, horizontal and vertical resolutions for ocean and sea ice models, initialized components/variables, reforecast period, ensemble members, and prediction lead months are described, respectively.

https://doi.org/10.5194/egusphere-2026-5070
Preprint. Discussion started: 31 August 2026

2.4. Diagnostic variables

We calculated anomaly correlation coefficients (ACCs; Murphy and Epstein, 1989) of the variables between the observation data and the model predictions. We also assess skill scores of persistence prediction based on observations by calculating anomaly correlation of the variables between the observation data for the initial and predicted months. We defined skillful predictions as the case in which the ACCs based on model prediction are statistically significant at a 95 % confidence level using Student's *t*-test and exceed the ACCs based on the persistence prediction. We performed regression analysis using the standardized Barents-Kara Sea SIE index which is defined as the SIE anomalies in the Barents-Kara Sea normalized by one standard deviation (σ). We also calculated zonal and meridional advection of SIT by sea ice velocity in the models. Also, we calculate the zonal heat transport vertically integrated at the Barents Sea Opening (BSO; 21ºE, 70-78ºN) between Svalbard and Norway, which is considered to be a key variable for the sea ice variability in the Barents Sea (Smedsrud et al., 2010; Wang et al., 2019).

3. Results

3.1. Predictability of summer Arctic sea ice

Eddy-permitting coupled models skillfully predict summer SIC in the Arctic Ocean, in particular, in the Barents-Kara Sea. Both the C3S multi-model ensemble mean (Fig. 2a) and the SINTEX-F3 ensemble mean (Fig. 2b) exhibit significantly positive anomaly correlations (ACCs; see Methods) for the SIC in the Barents-Kara Sea. The prediction skills for the multi-model ensemble mean C3S are generally higher than those for SINTEX-F3, likely due to cancellation of internal variability arising from the different model configurations. The spatial distribution of ACCs in the individual C3S models also resembles the one in SINTEX-F3 (Fig. S1), although the amplitude of ACCs differs across systems. Among the SINTEX-F model experiments (Fig. S2), F3-SI and F3-3DVAR (Fig. S2c, d) exhibit significantly high ACCs in the Barents-Kara Sea, while F2-SST and F3-SST (Fig. S2a, b) show little or no significant skill there. F3-SI performs slightly better than F3-3DVAR, suggesting that sea ice initialization plays a key role in skillful prediction of summer sea ice in the Barents-Kara Sea, while additional subsurface ocean initialization may partially degrade the benefits of sea ice initialization. Small differences between F2-SST and F3-SST also suggest that changes in model physics and resolutions alone provide limited benefits for this prediction target.

https://doi.org/10.5194/egusphere-2026-5070
Preprint. Discussion started: 31 August 2026

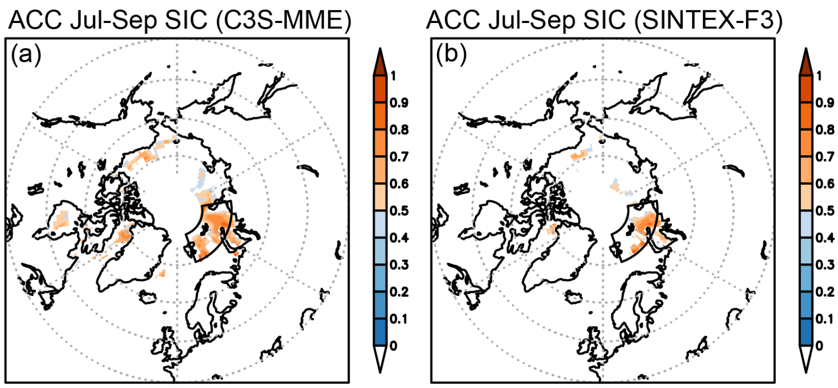

Figure 2: (a) ACC of July-September mean SIC during 1993-2016 between the observation (NSIDC) and the multi-model ensemble mean C3S. Color indicates ACCs that are statistically significant at 95 % using Student's *t*-test and exceed the ACCs of the persistence prediction based on the observed SIC. Black curved box indicates the Barents-Kara Sea of interest. (b) Same as in (a), but for the ensemble mean SIC in SINTEX-F3 with three different ocean and sea ice initialization schemes.

The C3S multi-model ensemble mean (Fig. 3a) demonstrates skillful prediction of SIE in the Barents-Kara Sea from May through September. ECMWF, METEOFR, and UKMO represent statistically significant prediction skills above the persistence prediction (see Methods) during July-September. Although the SINTEX-F3 ensemble mean (Fig. 3a) shows significantly high prediction skills in July only, both F3-SI and F3-3DVAR (Fig. 3b) demonstrate skillful predictions of SIE in the Barents-Kara Sea from May through September. F3-SI outperforms both F3-SST and F3-3DVAR, reinforcing the conclusion that sea ice initialization is important for skillful summer prediction in the Barents-Kara Sea, while the subsurface ocean initialization disturbs the correct sea-ice initialization. Both F2-SST and F3-SST (Fig. 3b) show lower prediction skills than the persistence, indicating that SST-only initialization contributes little to summer sea ice prediction in this region. We obtain similar results for the prediction skills of SIA in the Barents-Kara Sea (Fig. S3), although there are some differences in the amplitudes of ACCs with SIC and SIE.

https://doi.org/10.5194/egusphere-2026-5070
Preprint. Discussion started: 31 August 2026

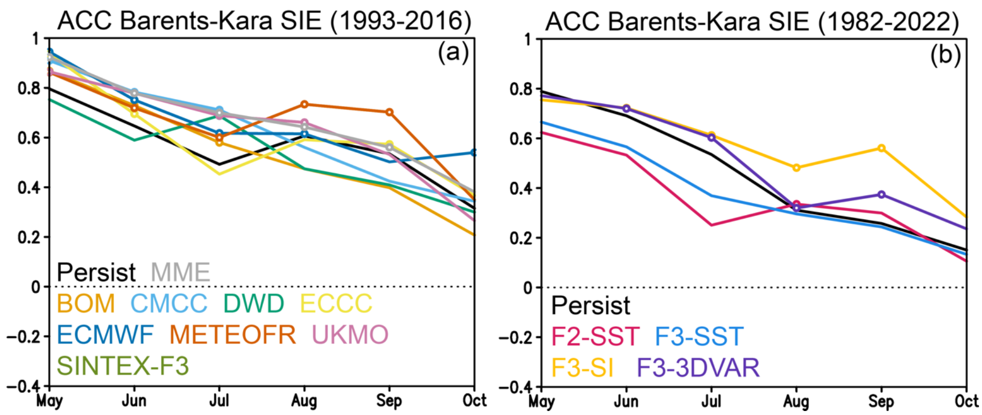

Figure 3: (a) ACC of Barents-Kara SIE (averaged over a black curved box in Fig. 1a) during 1993-2016 between the observation (NSIDC) and the predictions from the multi-model ensemble mean C3S (MME-C3S) and the ensemble mean BOM, CMCC, DWD, ECCC, ECMWF, METEOFR, UKMO, and SINTEX-F3, respectively. Skill scores of persistence prediction are shown in black. Open circles indicate ACCs that are statistically significant at 95 % using Student's *t*-test and exceed the ACCs of the persistence prediction based on the observed SIE. (b) Same as in (a), but for the ensemble mean SIE during 1982-2022 in SINTEX-F2 with SST initialization (F2-SST), SINTEX-F3 with SST initialization (F3-SST), SINTEX-F3 with SST and sea ice initializations (F3-SI), and SINTEX-F3 with SST, sea ice, and subsurface ocean initializations using 3DVAR approach (F3-3DVAR).

3.2. Physical processes underlying skillful prediction of summer sea ice in the Barents-Kara Sea

We regressed atmosphere, ocean, and sea ice variables onto the standardized SIE index in the Barents-Kara Sea (Fig. 4; See Methods). The observed SIE regression increases gradually towards summer (Fig. 4a). This evolution is associated with a gradual increase in negative SST regression in the Barents-Kara Sea (Fig. 4b), consistent with the close coupling between SIC and SST. F3-SST, F3-SI, and F3-3DVAR well capture the growth of the observed evolution of SIE and SST regressions, while F2-SST underestimates it.

https://doi.org/10.5194/egusphere-2026-5070
Preprint. Discussion started: 31 August 2026

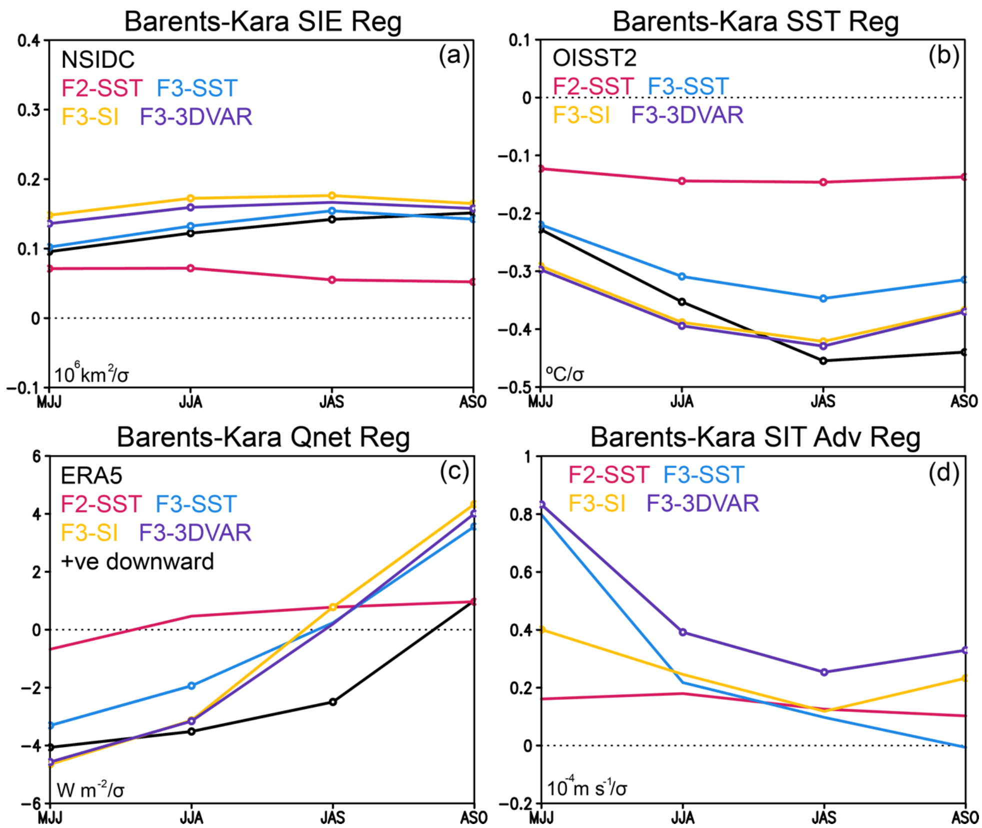

Figure 4: (a) Barents-Kara SIE anomalies (in 10^6 km^2/ σ) regressed on July-September mean standardized Barents-Kara SIE index (i.e., anomalies normalized by one standard deviation σ) during 1982-2022. The observation from NSIDC, the ensemble mean regressions from SINTEX-F2 with SST initialization (F2-SST), SINTEX-F3 with SST initialization (F3-SST), SINTEX-F3 with SST and sea ice initializations (F3-SI), and SINTEX-F3 with SST, sea ice, and subsurface ocean initializations using 3DVAR approach (F3-3DVAR) are shown, respectively. Here we show the slope of linear regression as the regression value on the Y-axis. Open circles indicate regression values that are statistically significant at 95 % using Student's *t*-test. (b) Same as in (a), but for Barents-Kara SST regressions (in ºC/ σ). The observation from OISSTv2 is shown as a reference. (c) Same as in (a), but for Barents-Kara net surface heat flux regressions (Qnet; in W m^{-2}/ σ). The reanalysis product from ERA5 is shown as a reference. Positive values indicate the heat goes into the ocean from the atmosphere. (d) Same as in (a), but for Barents-Kara SIT advection regressions (in 10^{-4} m s^{-1}/ σ). Positive values contribute to SIT growth.

https://doi.org/10.5194/egusphere-2026-5070
Preprint. Discussion started: 31 August 2026

Net surface heat flux regression in the Barents-Kara Sea (Fig. 4c) is significantly negative until July-September for the reanalysis and until June-August for F3-SST, F3-SI, and F3-3DVAR. The negative surface heat flux regression acts to cool the ocean and sea ice surface, thereby favoring larger SIE. Net shortwave radiation regression (Fig. 5a) contributes most to the net surface heat flux regression, consistent with a positive ice-albedo feedback: increased sea ice cover reflects more incoming solar radiation, which cools the surface and supports further sea ice retention. Net longwave radiation regression (Fig. 5b) is also significantly negative for the reanalysis and F2-SST, but its contributions to the net surface heat flux is comparatively small and very limited. In contrast, the contributions from the latent and sensible heat fluxes are positive to counteract the sea ice growth (Fig. 5c, d).

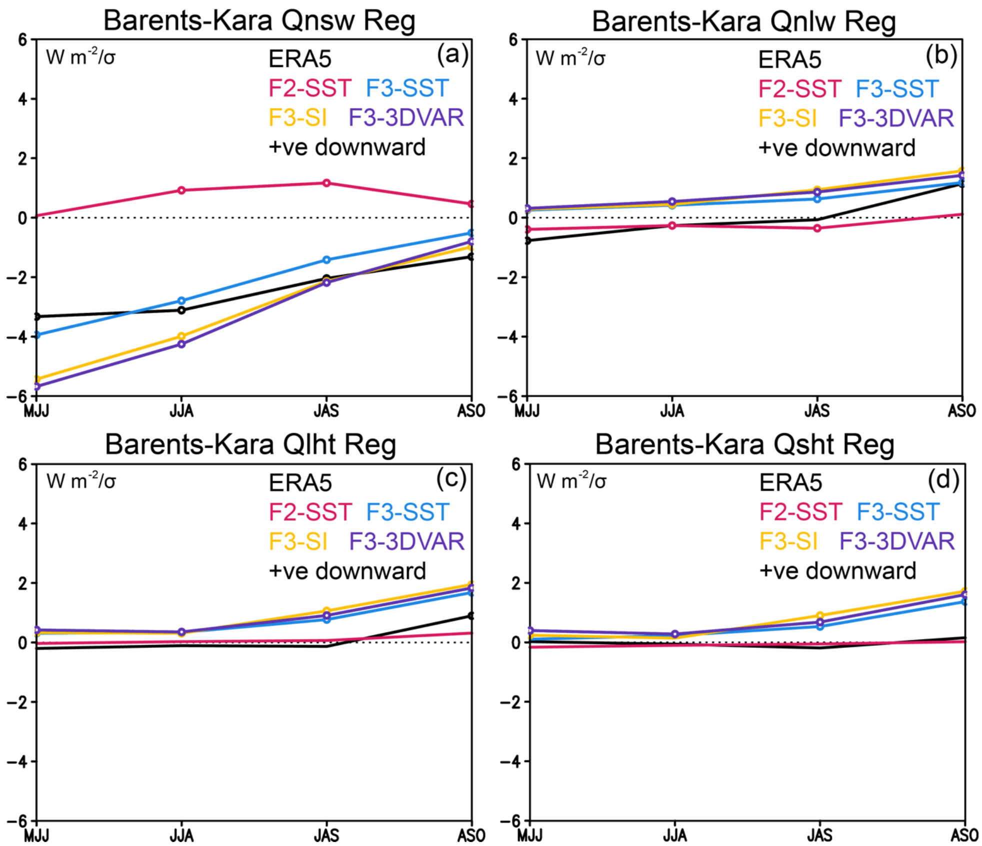

Figure 5: (a) Barents-Kara net shortwave radiation anomalies (Qnsw; in W m^{-2}/ σ) regressed on July-September mean standardized Barents-Kara SIE index during 1982-2022. The

https://doi.org/10.5194/egusphere-2026-5070
Preprint. Discussion started: 31 August 2026

reanalysis from ERA5, the ensemble mean regressions from SINTEX-F2 with SST initialization (F2-SST), SINTEX-F3 with SST initialization (F3-SST), SINTEX-F3 with SST and sea ice initializations (F3-SI), and SINTEX-F3 with SST, sea ice, and subsurface ocean initializations using 3DVAR approach (F3-3DVAR) are shown, respectively. Here we show the slope of linear regression as the regression value on the Y-axis. Open circles indicate regression values that are statistically significant at 95 % using Student's *t*-test. Positive values indicate the heat goes into the ocean from the atmosphere. (b-d) Same as in (a), but for Barents-Kara net longwave radiation (Qnlw), latent heat flux (Qlht), and sensible heat flux (Qsht) regressions (in W m^{-2}/ σ).

Horizontal advections of SIT (see Methods) in the Barents-Kara Sea show significantly positive regression values during May-July for F3-SST, F3-SI, and F3-3DVAR (Fig. 4d). Meridional advection (Fig. 6b) contributes more than zonal advection (Fig. 6a) to the total horizontal advection. In F3-SI, the advection of the SIT climatology by the meridional sea ice velocity anomaly (Fig. 6c) contributes the most to the total meridional advection, although both negative sea ice velocity (Fig. 6d) and positive meridional SIT gradient (Fig. 6e) regressions contribute to the meridional advection of SIT regression. These results indicate that thicker ice from higher latitudes is advected southward into the Barents-Kara Sea, supporting local sea ice persistence.

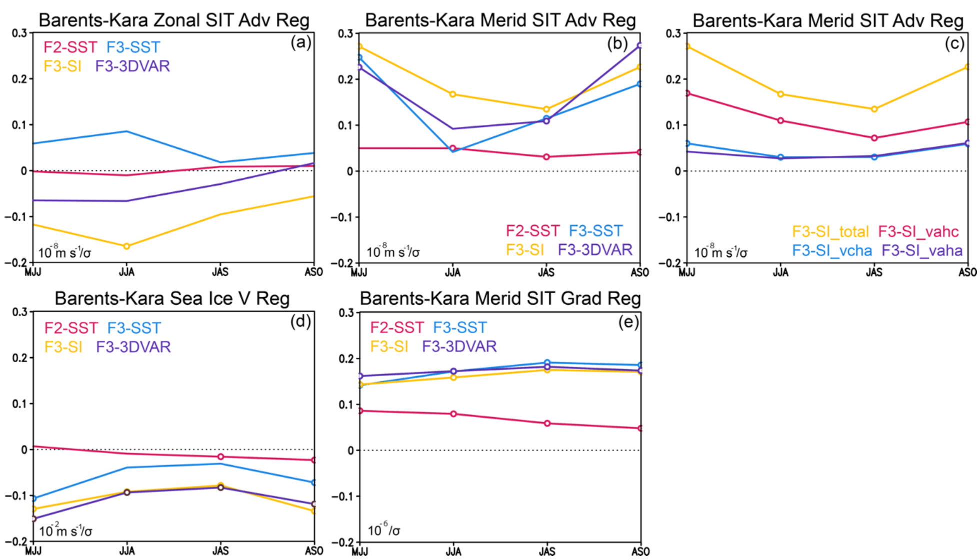

https://doi.org/10.5194/egusphere-2026-5070
Preprint. Discussion started: 31 August 2026

Figure 6: (a) Barents-Kara zonal SIT advection anomalies (in 10^{-8} m s^{-1}/σ) regressed on July-September mean standardized Barents-Kara SIE index during 1982-2022. The ensemble mean regressions from SINTEX-F2 with SST initialization (F2-SST), SINTEX-F3 with SST initialization (F3-SST), SINTEX-F3 with SST and sea ice initializations (F3-SI), and SINTEX-F3 with SST, sea ice, and subsurface ocean initializations using 3DVAR approach (F3-3DVAR) are shown, respectively. Here we show the slope of linear regression as the regression value on the Y-axis. Open circles indicate regression values that are statistically significant at 95 % using Student's *t*-test. Positive values contribute to SIT growth. (b-c) Same as in (a), but for Barents-Kara meridional SIT advection regressions and their components (in 10^{-8} m s^{-1}/σ). Regression values of the total meridional advection (total), the advection of the sea ice thickness climatology by the meridional sea ice velocity anomaly (vahc), the advection of the sea ice thickness anomaly by the meridional sea ice velocity climatology (vcha), and the advection of the sea ice thickness anomaly by the meridional sea ice velocity anomaly (vaha) are shown, respectively. (d-e) Same as in (a), but for Barents-Kara meridional sea ice velocity regressions (in 10^{-2} m s^{-1}/σ) and meridional SIT gradient regressions (in $10^{-6}/\sigma$).

The atmospheric reanalysis and the SINTEX-F model experiments show insignificant regression values for near-surface winds and wind curl over the Barents-Kara Sea (Fig. S4). Only F3-SST (Fig. S4a) shows significantly positive values of zonal winds, contributing to southward transport of thicker ice from higher latitudes. Only the reanalysis and F2-SST exhibit significantly negative wind curl, contributing to anomalous ice convergence in the region. Ocean salinity (Fig. S5a) and mixed-layer depth (Fig. S5b) regressions in the Barents-Kara Sea are insignificant in EN4, while they are significantly negative in F2-SST, F3-SST, F3-SI, and F3-3DVAR. Higher sea ice is associated with fresher near-surface water, reduced ocean density, and shallower mixed-layer.

In the subsurface ocean, the ocean temperature regression (Fig. 7) in the Barents-Kara Sea becomes significantly negative in summer, but in spring, only EN4 (Fig. 7a) shows insignificant ocean temperature regression, unlike the SINTEX-F model experiments (Fig. 7b-e). Ocean salinity (Fig. S6) also shows insignificant regression values for EN4 and SINTEX-F model experiments. Zonal heat transport vertically integrated at the Barents Sea Opening (Fig. S5c; see Methods) shows insignificant regression values for SINTEX-F model experiments. These results suggest that surface and subsurface ocean variability plays a weaker role than sea ice initialization in shaping seasonal predictability of summer sea ice in the Barents-Kara Sea.

https://doi.org/10.5194/egusphere-2026-5070
Preprint. Discussion started: 31 August 2026

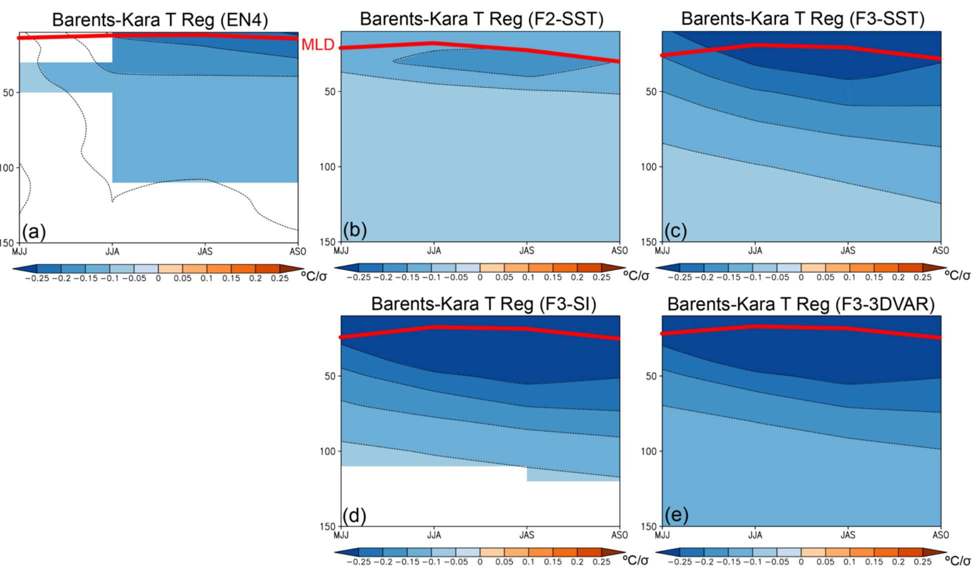

Figure 7: (a) Barents-Kara subsurface ocean temperature anomalies (T; in ºC/ σ) from EN4 regressed on July-September mean standardized Barents-Kara SIE index during 1982-2022. Color indicates regression values that are statistically significant at 95 % using Student's *t*-test. Red solid line corresponds to the mixed-layer depth (MLD) at which the ocean potential density increases by 0.03 kg m^{-3} from the one at 10 m depth. (b-e) Same as in (a), but for the ensemble mean regressions from SINTEX-F2 with SST initialization (F2-SST), SINTEX-F3 with SST initialization (F3-SST), SINTEX-F3 with SST and sea ice initializations (F3-SI), and SINTEX-F3 with SST, sea ice, and subsurface ocean initializations using 3DVAR approach (F3-3DVAR) are shown, respectively.

3.3. Potential sources of skillful prediction of summer sea ice in the Barents-Kara Sea

We regressed February-April mean Arctic SIT and SIC onto the standardized July-September mean Barents-Kara SIE index (See Methods). The sea ice reanalysis shows significantly positive SIT regression values in the Barents-Kara Sea (Fig. 8a). Both F2-SST (Fig. 8b) and F3-SST (Fig. 8c) reproduce this signal only weakly, whereas F3-SI (Fig. 8d) and F3-3DVAR (Fig. 8e) show substantially stronger positive SIT regression, consistent with the effect of sea ice initialization. We obtain similar results for the SIC regressions (Fig. S7). F3-SST (Fig. S7c) shows significantly positive SIC regression in the Barents-Kara Sea, while the improvement in initial SIT is much clearer in F3-SI and F3-3DVAR. This suggests that improved initialization of SIT from February to April is more important than that of SIC for capturing the subsequent

https://doi.org/10.5194/egusphere-2026-5070
Preprint. Discussion started: 31 August 2026

ice-albedo feedback and sea ice thickness advection that supports sea ice predictability from July to September.

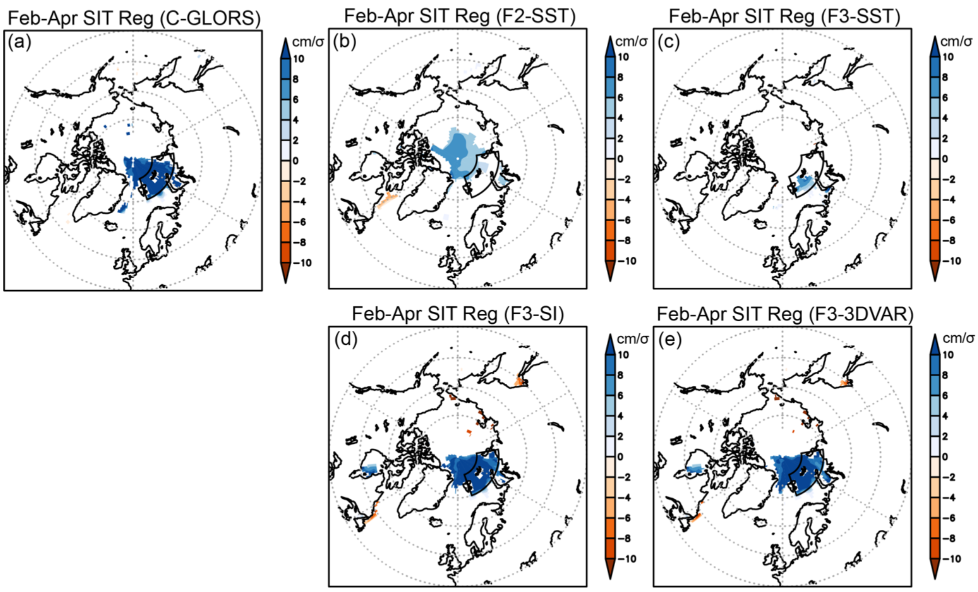

Figure 8: (a) February-April mean SIT anomalies (in cm/ σ) regressed on July-September mean standardized Barents-Kara SIE index during 1982-2022 from the C-GLORS reanalysis. Color indicates regression values that are statistically significant at 95 % using Student's *t*-test. (b-e) Same as in **a**, but for the ensemble mean SIT regressions from SINTEX-F2 with SST initialization (F2-SST), SINTEX-F3 with SST initialization (F3-SST), SINTEX-F3 with SST and sea ice initializations (F3-SI), and SINTEX-F3 with SST, sea ice, and subsurface ocean initializations using 3DVAR approach (F3-3DVAR).

4. Conclusion and Discussion

Using eddy-permitting coupled models from C3S and SINTEX-F3, this study has demonstrated overcoming barriers to predict summer sea ice in the Barents-Kara Sea from spring. SINTEX-F3 shows that sea ice initialization contributes more to this skill than ocean-only initializations. In particular, initializing sea ice conditions from February to Aprial improves the representation of initial SIT, which supports a more realistic evolution of the ice-albedo feedback and meridional sea ice advection from the higher latitudes. These processes appear to be central to the enhanced sea ice prediction skill in the Barents-Kara Sea from July to September. Ocean initializations have a more limited impact in our experiments. Summer

https://doi.org/10.5194/egusphere-2026-5070
Preprint. Discussion started: 31 August 2026

sea ice variability in the Barents-Kara Sea appears to be driven more strongly by the surface air-sea interaction (Bushuk et al., 2020) than by subsurface ocean variability (Onarheim et al., 2015), particularly as the ocean mixed layer shoals from spring to summer. Subsurface observational coverage remains sparse in the Arctic Ocean including the Barents-Kara Sea (Fig. 9), which likely constrains the quality of subsurface-ocean initialization.

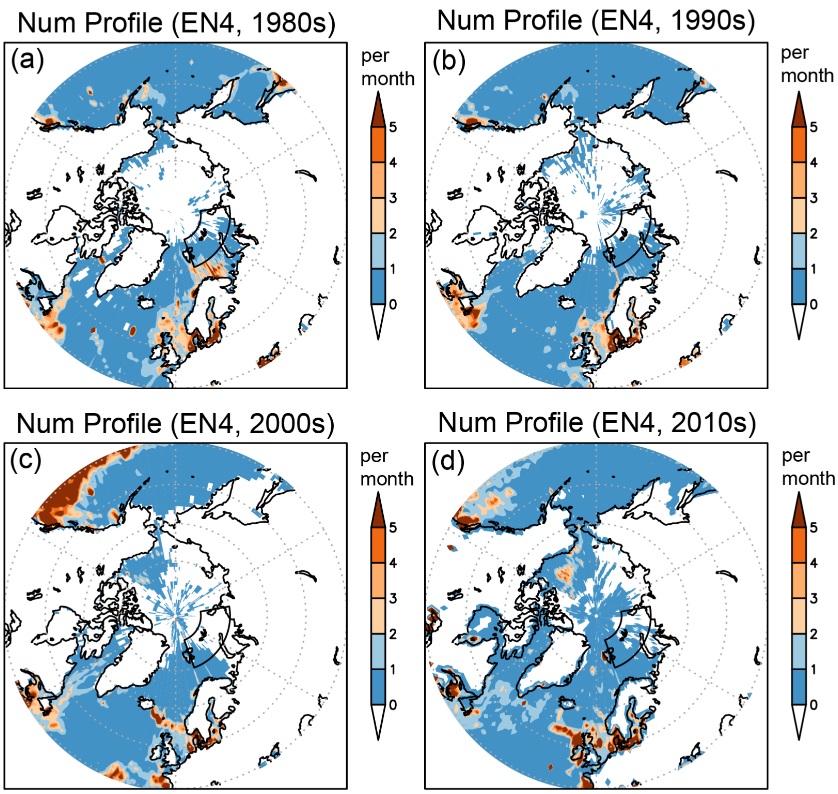

Figure 9: (a) Number of ocean observation profiles (color; in count per month) in the Arctic Ocean during the 1980s from EN4. (b-e), Same as in (a), but for the observation profiles from the 1990s to 2010s.

There is no denying the fact that atmospheric initialization adopted in most C3S models plays a role in skillful prediction of summer sea ice in the Barents-Kara Sea. Atmospheric initialization improves initial conditions of atmospheric temperature (Bushuk et al., 2019), surface heat flux, cloud or water vapor (Zeng et al., 2023) thereby improving initial sea ice conditions. This may lead to better representation of the subsequent ice-albedo feedback and horizontal sea ice transport in the coupled models, although we cannot verify these impacts

https://doi.org/10.5194/egusphere-2026-5070
Preprint. Discussion started: 31 August 2026

due to the limited availability of model output from C3S. Further comparison studies using C3S and SINTEX-F3 with atmospheric initialization are required and underway for better understanding the relative importance of sea ice and atmospheric initializations on the skillful prediction of summer sea ice in the Arctic Ocean.

This study has large implications for the necessity of long-term sea ice observation data. The SIC observation data derived from the satellite passive microwave have a long record from 1978 (DiGirolamo et al., 2022). The satellite-derived SIT data from the radar altimetry begins only in 2010 (Kurtz et al., 2017). Assimilating and initializing the SIT anomalies in a coupled model (Zhang et al., 2023) has proven useful for improving sea ice prediction skills in the Arctic Ocean. Since large mean-state differences in the SIT between observations and models can cause numerical instability or initial shock, and errors, anomaly-based SIT initialization may be a particular practical path forward (Zhang et al., 2023). These imply that the spring predictability barrier is not an intrinsic limit of the climate system, but arises from incomplete initialization of sea ice state variables in coupled models. Given these potential benefits, continued and extended SIT observations should help improve the prediction of summer sea ice in the Barents-Kara Sea.

Code Availability

All observational and modelling analyses were carried out using open-source Fortran and GrADS codes. Due to the large data size, only sample codes for the numerical analysis are provided here: https://doi.org/10.5281/zenodo.19660102. Additional analysis codes are also available from the corresponding author upon request.

Data Availability

Sea surface temperature data are available from NOAA: https://psl.noaa.gov/data/gridded/data.noaa.oisst.v2.highres.html. Subsurface ocean data are provided from UK Met Office: https://www.metoffice.gov.uk/hadobs/en4/. Sea ice concentration data are obtained from NSIDC: https://doi.org/10.5067/MPYG15WAA4WX. Sea ice thickness reanalysis is available from C-GLORS: http://c-glors.cmcc.it/index/index.html. Atmospheric reanalysis from ERA5 is downloaded from the Copernicus Climate Data Store: https://doi.org/10.24381/cds.f17050d7. The C3S seasonal forecasts are available from Copernicus Climate Data Store: https://doi.org/10.24381/cds.68dd14c3.

https://doi.org/10.5194/egusphere-2026-5070
Preprint. Discussion started: 31 August 2026

Author contribution

YM and TD carried out the model experiments. DI and AC provided the sea ice data for the model experiment, while AS developed the model code for the data assimilation. YM prepared the manuscript with contributions from all co-authors.

Competing interests

The authors declare that they have no conflict of interest.

Acknowledgments

We performed the SINTEX-F model experiments on Earth Simulator at JAMSTEC. We thank Drs. Alessandro Damiani, J. V. Ratnam, Ingo Richter, and Shuhei Masuda for providing constructive comments on the original research. The present research is supported by JSPS KAKENHI Grant Number 26K00786.

https://doi.org/10.5194/egusphere-2026-5070
Preprint. Discussion started: 31 August 2026

References

Balan-Sarojini, B., Tietsche, S., Mayer, M., Balmaseda, M., Zuo, H., de Rosnay, P., Stockdale, T., and Vitart, F.: Year-round impact of winter sea ice thickness observations on seasonal forecasts. *Cryosphere,* 15, 325–344, https://doi.org/10.5194/tc-15-325-2021, 2021.

Batté, L., Välisuo, I., Chevallier, M., Acosta Navarro, J. C., Ortega, P., and Smith, D.: Summer predictions of Arctic sea ice edge in multi-model seasonal re-forecasts. *Clim. Dyn.,* 54, 5013-5029, https://doi.org/10.1007/s00382-020-05273-8, 2020.

Blockley, E. W., and Peterson, K. A.: Improving Met Office seasonal predictions of Arctic sea ice using assimilation of CryoSat-2 thickness. *Cryosphere,* 12, 3419–3438, https://doi.org/10.5194/tc-12-3419-2018, 2018.

Bloom, S. C., Takacs, L. L., Da Silva, A. M., and Ledvina, D.: Data assimilation using incremental analysis updates. *Mon. Weather Rev.,* 124, 1256-1271, https://doi.org/10.1175/1520-0493(1996)124<1256:DAUIAU>2.0.CO;2, 1996.

Boé, J., Hall, A., and Qu, X.: September sea-ice cover in the Arctic Ocean projected to vanish by 2100. *Nat. Geo.,* 2, 341-343, https://doi.org/10.1038/ngeo467, 2009.

Bonan, D. B., Bushuk, M., and Winton, M.: A spring barrier for regional predictions of summer Arctic sea ice. *Geophys. Res. Lett.,* 46, 5937-5947, https://doi.org/10.1029/2019GL082947, 2019.

Bushuk, M., Msadek, R., Winton, M., Vecchi, G., Yang, X., Rosati, A., and Gudgel, R.: Regional Arctic sea–ice prediction: Potential versus operational seasonal forecast skill. *Clim. Dyn.,* 52, 2721-2743, https://doi.org/10.1007/s00382-018-4288-y, 2019.

Bushuk, M., Msadek, R., Winton, M., Vecchi, G. A., Gudgel, R., Rosati, A., and Yang, X.: Skillful regional prediction of Arctic sea ice on seasonal timescales. *Geophys. Res. Lett.,* 44, 4953-4964, https://doi.org/10.1002/2017GL073155, 2017.

https://doi.org/10.5194/egusphere-2026-5070
Preprint. Discussion started: 31 August 2026

Bushuk, M., Winton, M., Bonan, D. B., Blanchard-Wrigglesworth, E., and Delworth, T. L.: A mechanism for the Arctic sea ice spring predictability barrier. *Geophys. Res. Lett.,* 47, e2020GL088335, https://doi.org/10.1029/2020GL088335, 2020.

Bushuk, M., Yang, X., Winton, M., Msadek, R., Harrison, M., Rosati, A., and Gudgel, R.: The value of sustained ocean observations for sea ice predictions in the Barents Sea. *J. Climate,* 32, 7017-7035, https://doi.org/10.1175/JCLI-D-19-0179.1, 2019.

Cavalieri, D. J., and Parkinson, C. L.: Arctic sea ice variability and trends, 1979–2010. *Cryosphere,* 6, 881-889, https://doi.org/10.5194/tc-6-881-2012, 2012.

Christiansen, J. S., Mecklenburg, C. W., and Karamushko, O. V.: Arctic marine fishes and their fisheries in light of global change. *Glob. Change Biol.,* 20, 352-359, https://doi.org/10.1111/gcb.12395, 2014.

Cipollone, A., Banerjee, D. S., Iovino, D., Aydogdu, A., and Masina, S.: Bivariate sea-ice assimilation for global-ocean analysis–reanalysis. *Oce. Sci.,* 19, 1375–1392, https://doi.org/10.5194/os-19-1375-2023, 2023.

Day, J. J., Hawkins, E., and Tietsche, S. Will Arctic sea ice thickness initialization improve seasonal forecast skill?. *Geophys. Res. Lett.,* 41, 7566-7575, https://doi.org/10.1002/2014GL061694, 2014b.

Day, J. J., Tietsche, S., and Hawkins, E.: Pan-Arctic and regional sea ice predictability: Initialization month dependence. *J. Climate,* 27, 4371-4390, https://doi.org/10.1175/JCLI-D-13-00614.1, 2014a.

DiGirolamo, N. E., Parkinson, C. L., Cavalieri, D. J., Gloersen, P., and Zwally, H. J.: Sea Ice Concentrations from Nimbus-7 SMMR and DMSP SSM/I-SSMIS Passive Microwave Data, Version 2. Boulder, Colorado USA. NASA National Snow and Ice Data Center Distributed Active Archive Center. https://doi.org/10.5067/MPYG15WAA4WX, 2022.

https://doi.org/10.5194/egusphere-2026-5070
Preprint. Discussion started: 31 August 2026

Dirkson, A., Merryfield, W. J., and Monahan, A.: Impacts of sea ice thickness initialization on seasonal Arctic sea ice predictions. *J. Climate,* 30, 1001-1017, https://doi.org/10.1175/JCLI-D-16-0437.1, 2017.

Diro, G. T. et al.: The Canadian Seasonal to Interannual Prediction System version 3.0 (CanSIPSv3,0). Canadian Meteorological and Environmental Prediction Centre technical note, Environment and Climate Change, Canada. https://collaboration.cmc.ec.gc.ca/cmc/cmoi/product_guide/docs/tech_notes/technote_cansips-300_20240611_e.pdf, 2024.

Fichefet, T., and Maqueda, M. M.: Sensitivity of a global sea ice model to the treatment of ice thermodynamics and dynamics. *J. Geophys. Res. Oce.,* 102, 12609-12646, https://doi.org/10.1029/97JC00480, 1997.

Fröhlich, K. et al.: The German Climate Forecast System: GCFS2. Earth and Space Science Open Archive, 282. https://doi.org/10.1002/essoar.10502582.1, 2020.

Giorgetta, M. A., Roeckner, E., Mauritsen, T., Bader, J., Crueger, T., Esch, M., Rst, S., Kornblueh, L., Schmidt, H., Kinne, S., Hohenegger, C., Möbis, B., Krismer, T., Wieners, K. -H., and Stevens, B.: The atmospheric general circulation model ECHAM6-model description, Berichte zur Erdsystemforschung / Max-Planck-Institut für Meteorologie, 135, 177 pp, 2013.

Good, S. A., Martin, M. J., and Rayner, N. A.: EN4: quality controlled ocean temperature and salinity profiles and monthly objective analyses with uncertainty estimates. *J. Geophys. Res. Oce.,* 118, 6704–6716, https://doi.org/10.1002/2013JC009067, 2013.

Guemas, V. et al.: A review on Arctic sea-ice predictability and prediction on seasonal to decadal time-scales. *Q. J. R. Meteorl. Soc.,* 142, 546-561, https://doi.org/10.1002/qj.2401, 2016.

Guemas, V., Chevallier, M., Déqué, M., Bellprat, O., and Doblas-Reyes, F.: Impact of sea ice initialization on sea ice and atmosphere prediction skill on seasonal timescales. *Geophys. Res. Lett.,* 43, 3889-3896, https://doi.org/10.1002/2015GL066626, 2016.

Hersbach, H. et al.: The ERA5 global reanalysis. *Q. J. R. Meteorol. Soc.*, 146, 1999–2049, https://doi.org/10.1002/qj.3803, 2020.

Holland, M. M., and Hunke, E. C.: A review of Arctic sea ice climate predictability in large-scale Earth system models. *Oceanogr.,* 35, 20-27, https://doi.org/10.5670/oceanog.2022.113, 2022.

Jahn, A., Holland, M. M., and Kay, J. E.: Projections of an ice-free Arctic Ocean. *Nat. Rev. Earth Env.,* 5, 164-176, https://doi.org/10.1038/s43017-023-00515-9, 2024.

Kurtz, N., and Harbeck, J.: CryoSat-2 Level-4 Sea Ice Elevation, Freeboard, and Thickness, Version 1. Boulder, Colorado USA. NASA National Snow and Ice Data Center Distributed Active Archive Center. https://doi.org/10.5067/96JO0KIFDAS8, 2017.

Lannuzel, D. et al.: The future of Arctic sea-ice biogeochemistry and ice-associated ecosystems. *Nat. Clim. Change*, 10, 983-992, https://doi.org/10.1038/s41558-020-00940-4, 2020.

Levitus, S.: Climatological atlas of the world ocean (Vol. 13), US Department of Commerce, National Oceanic and Atmospheric Administration, NOAA/ERL GFDL Professional Paper 13, Princeton, N.J., 173 pp, 1982.

Liu, A. et al.: Assimilating summer sea ice thickness enhances predictions of Arctic sea ice and surrounding atmosphere within two months. *npj Clim. Atmos. Sci.,* 8, 210, https://doi.org/10.1038/s41612-025-01050-8, 2025.

Locarnini, R. A., Mishonov, A.V., Antonov, J. I., Boyer, T. P., Garcia, H. E., Baranova, O. K., Zweng, M. M., Paver, C. R., Reagan, J. R., Johnson, D. R., Hamilton, M., & Seidov, D.: *World Ocean Atlas 2013, Volume 1: Temperature.* S. Levitus, Ed., A. Mishonov Technical Ed.; NOAA Atlas NESDIS 73, 40 pp, 2013.

Madec, G.: NEMO ocean engine, Note du Pole de modélisation, Institut Pierre-Simon Laplace (IPSL), France. No 27. ISSN No 1288-1619, 2008.

https://doi.org/10.5194/egusphere-2026-5070
Preprint. Discussion started: 31 August 2026

Madec, G. et al.: NEMO ocean engine, Scientific Notes of Climate Modelling Center, 27 — ISSN 1288-1619, Institut Pierre-Simon Laplace (IPSL). https://doi.org/10.5281/zenodo.1464816, 2019.

Masson, S., Terray, P., Madec, G., Luo, J. J., Yamagata, T., and Takahashi, K.: Impact of intra-daily SST variability on ENSO characteristics in a coupled model. *Clim. Dyn.,* 39, 681-707, https://doi.org/10.1007/s00382-011-1247-2, 2012.

Massonnet, F., Fichefet, T., Goosse, H., Vancoppenolle, M., Mathiot, P., and König Beatty, C.: On the influence of model physics on simulations of Arctic and Antarctic sea ice. *Cryosphere,* 5, 687-699, https://doi.org/10.5194/tc-5-687-2011, 2011.

Meier, W. N. et al.: Arctic sea ice in transformation: A review of recent observed changes and impacts on biology and human activity. *Rev. Geophys.* 52, 185-217, https://doi.org/10.1002/2013RG000431, 2014.

Melia, N., Haines, K., and Hawkins, E. Sea ice decline and 21st century trans-Arctic shipping routes. *Geophys. Res. Lett.,* 43, 9720-9728, https://doi.org/10.1002/2016GL069315, 2016.

Murphy, A. H., and Epstein, E. S.: Skill scores and correlation coefficients in model verification. *Mon. Weather Rev.,* 117, 572-582, https://doi.org/10.1175/1520-0493(1989)117<0572:SSACCI>2.0.CO;2, 1989.

Nordeng, T. E.: Extended versions of the convective parametrization scheme at ECMWF and their impact on the mean and transient activity of the model in the tropics, Research Department Technical Memorandum, 206, 1-41, https://doi.org/10.21957/e34xwhysw, 1994.

Notz, D., and Community, S. I. M. I. P. Arctic sea ice in CMIP6. *Geophys. Res. Lett.,* 47, e2019GL086749, https://doi.org/10.1029/2019GL086749, 2020.

Onarheim, I. H., Eldevik, T., Årthun, M., Ingvaldsen, R. B., and Smedsrud, L. H.: Skillful prediction of Barents Sea ice cover. *Geophys. Res. Lett.,* 42, 5364-5371, https://doi.org/10.1002/2015GL064359, 2015.

https://doi.org/10.5194/egusphere-2026-5070
Preprint. Discussion started: 31 August 2026

Ono, J., Komuro, Y., and Tatebe, H.: Impact of sea-ice thickness initialized in April on Arctic sea-ice extent predictability with the MIROC climate model. *Ann. Glaciol.,* 61, 97-105, https://doi.org/10.1017/aog.2020.13, 2020.

Palma, D. et al.: Cruising the marginal ice zone: Climate change and Arctic tourism. *Polar Geography,* 42, 215-235, https://doi.org/10.1080/1088937X.2019.1648585, 2019.

Raddatz, T. J., Reick, C. H., Knorr, W., Kattge, J., Roeckner, E., Schnur, R., Wetzel, P., and Jungclaus, J.: Will the tropical land biosphere dominate the climate–carbon cycle feedback during the twenty-first century? *Clim. Dyn.,* 29, 565-574. https://doi.org/10.1007/s00382-007-0247-8, 2007.

Reynolds, R. W., Rayner, N. A., Smith, T. M., Stokes, D. C., and Wang, W.: An improved in situ and satellite SST analysis for climate. *J. Climate,* 15, 1609-1625, https://doi.org/10.1175/1520-0442(2002)015<1609:AIISAS>2.0.CO;2, 2002.

Reynolds, R. W., Smith, T. M., Liu, C., Chelton, D. B., Casey, K. S., and Schlax M. G.: Daily High-Resolution-Blended Analyses for Sea Surface Temperature. *J. Climate,* 20, 5473-5496, https://doi.org/10.1175/2007JCLI1824.1, 2007.

Roeckner, E. et al.: The atmospheric general circulation model ECHAM 5. PART I: Model description, Max Planck Institute for Meteorology, 349, ISSN 0937-1060, 2003.

Selivanova, J., Iovino, D., and Cocetta, F. Past and future of the Arctic sea ice in High-Resolution Model Intercomparison Project (HighResMIP) climate models. *Cryosphere,* 18, 2739-2763, https://doi.org/10.5194/tc-18-2739-2024, 2024.

Sanna, A. et al.: CMCC Technical Note n.301. https://doi.org/10.25424/cmcc-dkcv-fs25, 2025.

Sasaki, W., Richards, K. J., and Luo, J. J.: Impact of vertical mixing induced by small vertical scale structures above and within the equatorial thermocline on the tropical Pacific in a CGCM. *Clim. Dyn.,* 41, 443-453, https://doi.org/10.1007/s00382-012-1593-8, 2013.

Song, R., Mu, L., Loza, S. N., Kauker, F., and Chen, X.: Assimilating summer sea-ice thickness observations improves Arctic sea-ice forecast. *Geophys. Res. Lett.,* 51, e2024GL110405, https://doi.org/10.1029/2024GL110405, 2024.

Stockdale, T.: SEAS5 User Guide. ECMWF. https://www.ecmwf.int/en/elibrary/81237-seas5-user-guide, 2021.

Storto, A., and Masina, S.: C-GLORSv5: an improved multipurpose global ocean eddy-permitting physical reanalysis. *Ear. Syst. Sci. Data,* 8, 679–696, https://doi.org/10.5194/essd-8-679-2016, 2016.

Storto, A., Oddo, P., Cipollone, A., Mirouze, I., and Lemieux-Dudon, B.: Extending an oceanographic variational scheme to allow for affordable hybrid and four-dimensional data assimilation. *Oce. Model.,* 128, 67-86, https://doi.org/10.1016/j.ocemod.2018.06.005, 2018.

Smedsrud, L. H., Ingvaldsen, R., Nilsen, J. Ø., and Skagseth, Ø.: Heat in the Barents Sea: Transport, storage, and surface fluxes. *Oce. Sci.* 6, 219-234, https://doi.org/10.5194/os-6-219-2010, 2010.

Specq, D., Dorel, L., Beuvier, J., Ardilouze, C., and Batté, L.: Documentation of the Météo-France seasonal forecasting system 9. Zenodo. https://doi.org/10.5281/zenodo.15861483, 2025.

Valcke, S.: The OASIS3 coupler: a European climate modelling community software. *Geosci. Mod. Dev.* 6, 373–388. https://doi.org/10.5194/gmd-6-373-2013, 2013.

Valcke, S., Caubel, A., Vogelsang, R., and Declat, D.: OASIS3 User's Guide (oasis3 prism 2-4), PRISM Report No 2, 5th Ed., CERFACS, Toulouse, France, 2004.

Vancoppenolle, M., Rousset, C., Blockley, E., & the NEMO Sea Ice Working Group.: SI3 – Sea Ice modelling Integrated Initiative – The NEMO Sea Ice Engine, Zenodo. https://doi.org/10.5281/zenodo.7534900, 2023.

Vihma, T.: Effects of Arctic sea ice decline on weather and climate: A review. *Surv. Geophys.,* 35, 1175-1214, https://doi.org/10.1007/s10712-014-9284-0, 2014.

Wang, C. et al.: Recent slowing of Arctic sea ice melt tied to multidecadal NAO variability. *Nat. Comm.,* 16, 8504, https://doi.org/10.1038/s41467-025-63520-0, 2025.

Wang, M., and Overland, J. E.: A sea ice free summer Arctic within 30 years?. *Geophys. Res. Lett.,* 36, L07502, https://doi.org/10.1029/2009GL037820, 2009.

Wang, M., and Overland, J. E.: A sea ice free summer Arctic within 30 years: An update from CMIP5 models. *Geophys. Res. Lett.,* 39, L18501, https://doi.org/10.1029/2012GL052868, 2012.

Wang, Q. et al.: Ocean heat transport into the Barents Sea: Distinct controls on the upward trend and interannual variability. *Geophys. Res. Lett.,* 46, 13180-13190, https://doi.org/10.1029/2019GL083837, 2019.

Wedd, R. et al.: ACCESS-S2: the upgraded Bureau of Meteorology multi-week to seasonal prediction system. *J. South. Hemisph. Earth Syst. Sci.,* 72, 218–242, https://ui.adsabs.harvard.edu/link_gateway/2022JSHES..72..218W/doi:10.1071/ES22026, 2022.

Williams, K. D. et al.: The Met Office Global Coupled model 3.0 and 3.1 (GC3.0 and GC3.1) configurations. *J. Adv. Model. Earth Syst.,* 10, 357–380, https://doi.org/10.1002/2017MS001115, 2017.

Zeng, J., Yang, Q., Li, X., Yuan, X., Bushuk, M., and Chen, D.: Reducing the spring barrier in predicting summer Arctic sea ice concentration. *Geophys. Res. Lett.,* 50, e2022GL102115, https://doi.org/10.1029/2022GL102115, 2023.

Zhang, J.: Recent slowdown in the decline of Arctic sea ice volume under increasingly warm atmospheric and oceanic conditions. *Geophys. Res. Lett.,* 48, e2021GL094780, https://doi.org/10.1029/2021GL094780, 2021.

Zhang, R.: Mechanisms for low-frequency variability of summer Arctic sea ice extent. *Proc. Nat. Aca. Sci.,* 112, 4570-4575, https://doi.org/10.1073/pnas.1422296112, 2015.

Zhang, Y. F., Bushuk, M., Winton, M., Hurlin, B., Gregory, W., Landy, J., and Jia, L.: Improvements in september arctic sea ice predictions via assimilation of summer CryoSat-2 sea ice thickness observations. *Geophys. Res. Lett.,* 50, e2023GL105672, https://doi.org/10.1029/2023GL105672, 2023.

Zweng, M. M, Reagan, J. R., Antonov, J. I., Locarnini, R. A., Mishonov, A. V., Boyer, T. P. Garcia, H. E., Baranova, O. K., Johnson, D. R., Seidov, D., and Biddle, M. M.: *World Ocean Atlas 2013, Volume 2: Salinity*, S. Levitus, Ed., A. Mishonov Technical Ed.; NOAA Atlas NESDIS 74, 39 pp, 2013.